Solution and Solid-State Studies of Alkali Metal Aggregate Assemblies

John Jacob Morris

Publication Date

07-04-2008

CHAPTER 4

SYSTEMATIC STUDY OF 2,4,6-TRISUBSTITUTED ALKALI METAL ARYLOXIDES AGGREGATES HIGHLIGHTED BY THEIR USE IN HIGH-CONNECTIVITY NETWORKS

4.1 Introduction

One of the paradigms that emerged from the work presented in the previous chapter was that smaller, *i.e.* dimeric, aggregates can successfully be used as SBUs in the construction of extended coordination frameworks. This is in contrast to the previous work in our group that looked at using larger tetrameric and hexameric aggregates as SBUs.[1] The appeal of using dimeric aggregates as SBUs is that the smaller number of M-O_{Ar} bonds potentially allows an increase in the number of M-O_{solv} bonds. This could lead to exciting new possibilities for network topologies when a divergent linker, like dioxane, is used. We became interested in expanding on the work in the previous chapter by targeting the use of dimeric aryloxide aggregates as SBUs in combination with the heavier alkali metals. Therefore, our initial approach will take advantage of aryloxide ligands that have proven successful in our lithium aryloxide studies (Figure 4.1)

There are surprisingly few simple potassium aryloxide structures, all of which form discreet aggregates.[2] The size of the aggregates vary between monomeric and hexameric with the remaining coordination environment of the potassium atoms filled by

a Lewis base interaction with THF, pyridine, or non-deprotonated phenol. In a few of the structures the coordination environment is further filled through π-interactions with neighboring aryl rings of phenoxide.[2a,d] There are fewer simple rubidium and cesium aryloxide structures reported.[3]

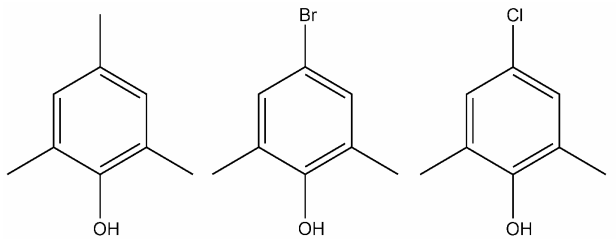

Figure 4.1 2,4,6-Trisubstitued phenols highlighted in this chapter

The aim of this chapter is twofold: (i) to explore the molecular aggregation chemistry of 2,4,6-trisubstituted aryloxide ligands in combination with the heavier alkali metals, and (ii) to explore the viability of using these systems for the construction of high-connectivity networks. We reasoned that aggregates containing the larger alkali metals were appealing candidates as SBUs for high-connectivity systems since they should allow multiple sites for network extension (increased metal solvation) or perhaps produce larger aggregates. Both of these factors could lead to interesting or novel network topologies. A potential drawback is increase the ionic character of the metal could lead to dynamic mixtures of aggregates or the formation of insoluble polymers. Because of the complicated nature of the extended materials presented in this chapter, the work will be preceded by a relevant discussion of network topology and strategies for network representation.

4.2 Network Topology

A subject of central importance within the area of metal-organic frameworks and coordination polymers is the study of network topology, which precisely describes the structure of extended solid-state materials. This field ties together chemists focused on synthesis, materials science and crystallography, with physicists and mathematicians interested in fundamental aspects of topology such as non-Euclidean geometry.[4] The growing number of framework structures being reported has led to an increasing emphasis towards identifying and classifying their underlying topologies. This systematic enumeration has been greatly aided by the recent construction of searchable databases and computer programs designed for topological analysis.[5]

A compelling illustration of the importance of topological classification comes from the paradigm that a small number of high-symmetry topologies dominate the structures of framework materials.[6] For example, two of the most commonly encountered nets are the diamondoid net (**dia**) and the primitive cubic net (**pcu**), resulting from tetrahedral and octahedral nodes respectively.[7] A recent survey of the CSD showed that 20.7% of all three-dimensional nets have **dia** topology and 12.9% have **pcu** topology.[6] Thus, the almost limitless potential complexity of extended structures is simplified, bringing at least some level of predictability to the design of new materials. The bolded net abbreviations are from the RCSR database, which will be described shortly.

Networks formed with connectivities greater than six are very unusual, with the large majority adopting either the high symmetry 8-connected body-centered cubic (**bcu**) net or the 12-connected face-centered cubic (**fcu**) net.[8] High-connectivity nets that do not have the highest possible symmetry are extremely rare, with almost all of the examples

being low-symmetry 8-connected nets or multinodal nets.[9] In fact, there is only one reported example of an uninodal 7-connected net and no examples of uninodal 9-, 10- or 11-connected nets.[8a] Therefore, there is presently very little experimental data available to predict which, if any, of the many thousands of possible topologies will dominate for each of these nodal types. Furthermore, no general synthetic strategy has emerged to prepare such unusual nodal geometries.

There are two main issues when dealing with complicated high-connectivity nets. The first issue is that they are often very difficult to represent graphically. This is especially true for nets that do not have high symmetry. The second issue is relating high-connectivity nets to both previously published examples and theoretically derived nets. While also relevant for low-connectivity nets, the rare and complicated nature of high-connectivity nets puts an increased emphasis on this issue. Therefore, a number of strategies have been developed for dealing with these issues. Since these strategies will be used throughout the rest of the manuscript, they will be briefly outlined below along with their strengths and weaknesses.

4.2.1 Strategies For Network Representation

High-connectivity networks are routinely broken down into a simple ball-and-stick representation. The node, represented as a single ball, can either be an isolated metal atom or a polynuclear cluster.[8] Figure 4.2 shows an example of how the extended structure of an 8-connected complex described later in this chapter, **4.10**, is reduced to a ball and stick representation with **bcu** topology. Although the final representation gives no structural information about the localized structure, the power of this technique lies in

its ability to easily convey the underlying topology of the extended structure to the non-specialist.

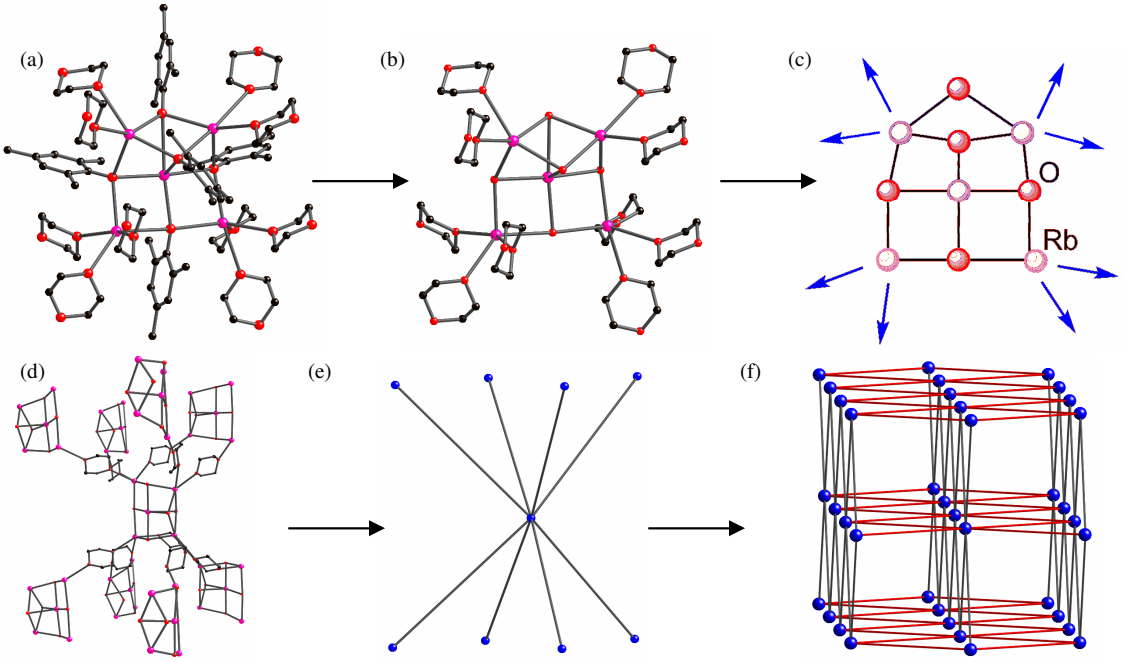

Figure 4.2 Stepwise deconstruction of the dioxane coordinated pentameric aggregate, **4.10**, showing (a) the full pentameric aggregate with ten coordinated dioxane molecules, (b) the aggregate with carbon atoms of the aryloxide removed for clarity, (c) illustration of the aggregate showing the eight unique points of network extension, (d) the pentameric aggregate linked to eight neighboring aggregates to give the **bcu** topology, (e) reduction of the pentameric aggregates and bridging dioxanes to ball and stick representation, (f) ball and stick view of **bcu** net.

Due to the complex nature of visualizing high-connectivity nets, a complimentary technique is to take the extended 3D net and described in terms of interconnected simpler subnets.[8a] An example of this is illustrated in Figure 4.2f in which the extended **bcu** topology of **4.10** can be shown as a parallel series of 4^4- nets (shown in red) that are intersected perpendicularly by another series of 4^4-nets (shown in gray). The strength of this approach is that even complex topologies can usually be reduced to simple 2D subnets such as the 4^4-, 6^3-, or 3^6-net and readily compared to other nets. For example the

6-connected **pcu** and 8-connected **bcu** net can both be simplified into parallel sheets of 4^4-subnets that are perpendicularly intersected by a similar series of 4^4-subnets. However, in the **pcu** net the perpendicular subnets intersect along the ring edges, whereas in the **bcu** net the subnets intersect across the face of the ring.

The major downside to the previous two approaches is that they give no formal classification about the extended structure. A more mathematical approach to describe nets is to use Schläfli, or topology, symbols, which describe the number and size of the shortest circuit at each angle of a vertex. Although a complete discussion of Schläfli symbols is beyond the scope of this work, a brief definition is adequate for understanding their role. Schläfli symbols describe the circuits at each vertex and have the form $A^a.B^b.C^c\ldots$ in which A<B<C and a+b+c = n(n-1)/2 for an n-coordinated vertex and signify the length (A, B, C) and number (a, b, c) of the shortest circuit contained in each of the angles. For example, the 4-coordinated diamond net (**dia**), which has 6 unique angles at each node with a 6-membered cirucuit at each angle, is given the Schläfli symbol 6^6. Likewise, the 6-coordinated primitive cubic network (**pcu**), with 15 unique angles, has twelve 4-membered circuits and three 6-membered circuits, and is given a Schläfli symbol of $4^{12}6^3$.

A complimentary mathematical approach to Schläfli symbols for describing topology is the td10 of a net, which is the cumulative sum of the first 10 shells of topological neighbors. For example, each node in the 6-connected **pcu** net has six topological neighbors in the first shell, eighteen in the second, thirty-eight in the third, *et cetera*, for a cummulative sum of the first ten shells of td10=1561. Related nets usually have similar values of td10, so this is a reliable way to find related nets of the same

coordination number. While the td10 of a net does not give the same amount of structural information as the Schläfli symbol it can still be a powerful tool for comparing nets. For example, the diamond net (**dia**) and lonsdaleite, or hexagonal diamond, net (**lon**) have the same Schläfli symbol of 6^6. The topology of the two nets are clearly different though, and this is shown by the td10 which is 981 for **dia** and 1027 for **lon**. When used together, the Schläfli symbol and the td10 give an accurate description of a net and simplifies the comparison of nets across the scientific disciplines.

Obviously, understanding the topology of a net is meaningless if it cannot be compared with previously published and theoretically calculated networks. Recently, two major online databases, the Reticular Chemistry Structure Resource (RCSR) and EPINET, have been created to help provide analysis and comparisons of network structures.[5] For example, the RSCR provides Schläfli symbols, the td10, and relevant references for known two- and three-dimensional nets. Each net in the RCSR is also given a three letter lowercase refcode for easy identification. This approach was chosen as a compliment to the zeolite databases, which use a three letter upper case refcode (e.g. FAU for faujasite).

4.3 Reactions of 4-(Cl/Br)-2,6-Dimethyphenol

4.3.1 Synthesis

The equimolar reaction of 4-Cl-2,6-dimethylphenol or 4-Br-2,6-dimethylphenol with NaH in 1,4-dioxane resulted in the instant formation of a precipitate, which dissolved on vigorous heating. High-quality crystals of both [(4-Cl-2,6-Me_2-

$C_6H_2ONa)_2\cdot(dioxane)_3]_\infty$ (**4.1**) and $[(4\text{-Br-}2,6\text{-}Me_2\text{-}C_6H_2ONa)_2\cdot(dioxane)_3]_\infty$ (**4.2**) were grown from the reaction solution after optimizing their concentrations and temperatures for crystal growth. Subsequent equimolar reactions of 4-Cl-2,6-dimethylphenol or 4-Br-2,6-dimethylphenol with KHMDS, RbHMDS, or CsHMDS under similar crystallization conditions gave high-quality crystals of $[(4\text{-Cl-}2,6\text{-}Me_2\text{-}C_6H_2OK)_2\cdot(dioxane)_{3.5}]_\infty$ (**4.3**), $[(4\text{-Br-}2,6\text{-}Me_2\text{-}C_6H_2OK)_2\cdot(dioxane)_{3.5}]_\infty$ (**4.4**), $[(4\text{-Cl-}2,6\text{-}Me_2\text{-}C_6H_2ORb)_2\cdot(dioxane)_{3.5}]_\infty$ (**4.5**), $[(4\text{-Br-}2,6\text{-}Me_2\text{-}C_6H_2ORb)_2\cdot(dioxane)_{3.5}]_\infty$ (**4.6**), and $[(4\text{-Cl-}2,6\text{-}Me_2\text{-}C_6H_2OCs)_7\cdot(dioxane)_1]_\infty$ (**4.7**). The following two subsections describe the molecular and extended structures of **4.1** - **4.7**. Because of the unique structure of **4.7**, its local and extended structure is described together in the extended structure section (section 4.3.3).

4.3.2 Molecular Structures

For our initial studies in using the heavier alkali metal aryloxide aggregates as SBUs in the design of high-connectivity networks, we were interested in expanding on the lithium 4-Cl/Br-2,6-dimethylphenoxide system (**3.1** and **3.2**) described in the previous chapter. Both lithium dimers possess two well-defined potential points of extension from each metal, i.e., two donor solvents per lithium. We reasoned that if a larger alkali metal was employed, with the aggregate remaining dimeric, each metal could be coordinated by a larger number of linkers giving rise to high-connectivity extended networks with rare, or even new, topologies.

High quality crystals of the sodium analogue of both phenols, $[(4\text{-Cl-}2,6\text{-}Me_2\text{-}C_6H_2ONa)_2\cdot(dioxane)_3]_\infty$ (**4.1**) and $[(4\text{-Br-}2,6\text{-}Me_2\text{-}C_6H_2ONa)_2\cdot(dioxane)_3]_\infty$ (**4.2**) were grown from dioxane solutions. Because the complexes are isostructural, only the

molecular and extended structure of **4.1** will be discussed. Important bond lengths and angles for both complexes are listed in Table 4.1.

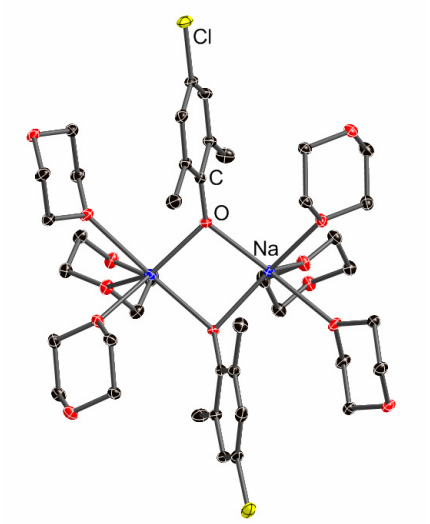

Figure 4.3 Dimeric aggregate of **4.1** coordinated by six divergent dioxane molecules. Hydrogen atoms are removed for clarity.

The aggregate of **4.1** is composed of a dimeric alkali metal aryloxide ring solvated by six dioxane molecules (Figure 4.3). The formation of a dimeric aggregate was expected because of the combination of an electron-withdrawing substituent at the *para*-position of the aryloxide ring and methyl groups at the *ortho*-position.[1] Similar to the dimeric lithium complex **3.1**, both sodiums in the dimer are symmetrically coordinated by dioxane. However, the larger sodium centers are now each coordinated by three dioxane molecules.The Na-O_{diox} bond distances are slightly longer at 2.267(1) – 2.515(1) Å than the Na-O_{Ar} distances of 2.221(1) – 2.239(1) Å.

High quality crystals of the potassium and rubidium analogues of both phenols, $[(4\text{-Cl-2,6-Me}_2\text{-C}_6\text{H}_2\text{OK})_2\cdot(\text{dioxane})_{3.5}]_\infty$ (**4.3**), $[(4\text{-Br-2,6-Me}_2\text{-C}_6\text{H}_2\text{OK})_2\cdot(\text{dioxane})_{3.5}]_\infty$ (**4.4**), $[(4\text{-Cl-2,6-Me}_2\text{-C}_6\text{H}_2\text{ORb})_2\cdot(\text{dioxane})_{3.5}]_\infty$ (**4.5**), and $[(4\text{-Br-2,6-Me}_2\text{-C}_6\text{H}_2\text{ORb})_2\cdot(\text{dioxane})_{3.5}]_\infty$ (**4.6**), were grown from dioxane solutions. Interestingly, all

four complexes are isostructural so only the molecular structure of **4.3** and **4.5** will be discussed.

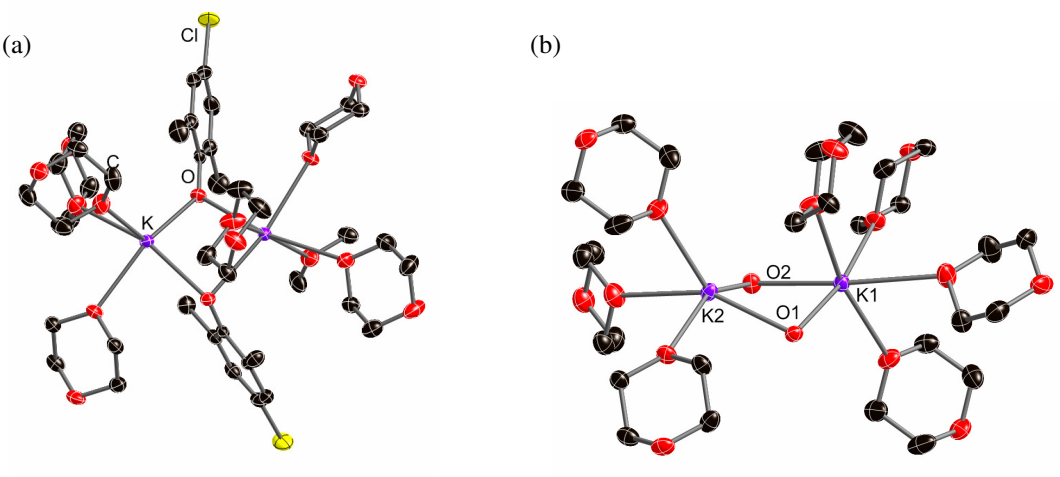

Figure 4.4 (a) Full dimeric aggregate of **4.3** with seven coordinated dioxane, and (b) the dimeric aggregate of **4.3** with carbon atoms of the aryloxide removed for clarity. Hydrogen atoms in both representations are removed for clarity.

The aggregate of **4.3** is composed of a dimeric alkali metal aryloxide ring solvated by seven dioxane molecules (Figure 4.4). The dimer is asymmetrically solvated, with K1 coordinated by four dioxane molecules, whereas K2 is coordinated by three dioxanes. The mean K1-$O_{(diox)}$ distance of 2.823 Å is substantially longer than the mean K2-$O_{(diox)}$ distance of 2.742 Å as a result of the increased steric crowding from the additional dioxane molecule and increased coordination number at the metal. In addition, the mean K1-$O_{(Ar)}$ distance of 2.674 Å, which is 0.08 Å longer than the K2-$O_{(Ar)}$ distance.

The rubidium analogue **4.5** forms a similar dimeric aggregate that is asymmetrically coordinated by seven dioxane molecules (Figure 4.5). As was seen in **4.3**, the mean Rb1-$O_{(diox)}$ distance of 2.927 Å, for the rubidium with four dioxanes coordinated, is longer than the mean Rb2-$O_{(diox)}$ distance of 2.870 Å. Similarly, the mean Rb(1)-$O_{(Ar)}$ distance of 2.808 Å is longer than the mean Rb(2)-$O_{(Ar)}$ distance of 2.720 Å.

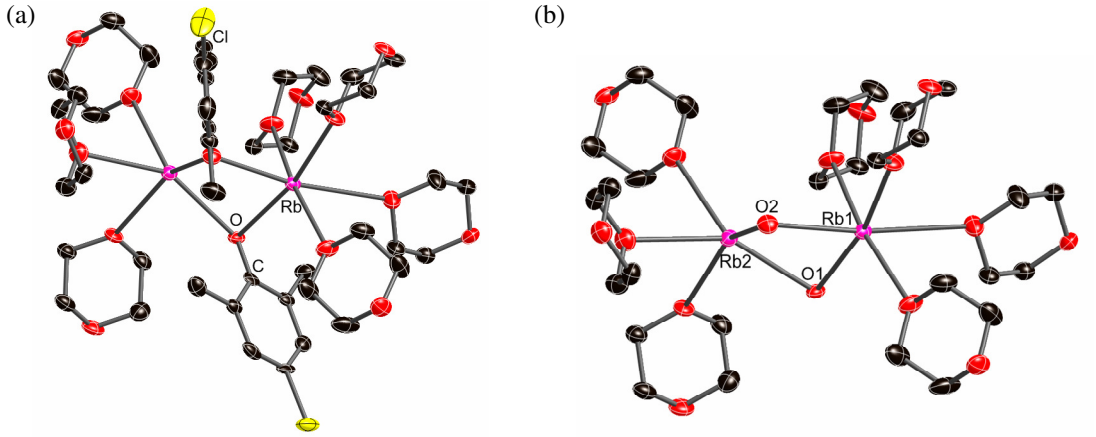

Figure 4.5 (a) Full dimeric aggregate of **4.5** with seven coordinated dioxane, and (b) the dimeric aggregate of **4.5** with carbon atoms of the aryloxide removed for clarity. Hydrogen atoms in both representations are removed for clarity.

TABLE 4.1

KEY BONDS LENGTHS [Å] AND ANGLES (°) FOR **4.1**-**4.12.** MEAN VALUES ARE IN BRACKETS

	M-O_{Ar}	**M-$O_{Solv.}$**	**M-O-M**	**O-M-O**
4.1	2.221(1) – 2.391(1)	2.267(1) – 2.515(1)	91.50(4), 96.89(5)	85.45(4), 85.50(4)
(M=Na)	<2.306>	<2.389>		
4.2	2.247(7) – 2.328(7)	2.278(7) – 2.499(7)	95.8(3), 95.9(3)	84.0(2), 84.1(2)
(M=Na)	<2.228>	<2.398>		
4.3	2.555(1) – 2.736(1)	2.715(2) – 2.886(2)	87.22(4), 91.59(4)	83.72(4), 86.96(4)
(M=K)	<2.634>	<2.788>		
4.4	2.560(2) – 2.730(2)	2.702(2) – 2.879(2)	88.07(6), 92.34(6)	83.08(6), 86.00(6)
(M=K)	<2.631>	<2.794>		
4.5	2.673(3) – 2.863(3)	2.854(3) – 2.986(4)	84.31(9), 88.29(1)	85.8(1), 89.4(1)
(M=Rb)	<2.764>	<2.903>		
4.6	2.668(2) – 2.838(2)	2.840(3) – 2.976(2)	85.42(5), 89.17(5)	85.34(5), 88.35(6)
(M=Rb)	<2.745>	<2.889>		
4.7	2.781(3) – 3.401(3)	—	88.32(7) – 152.44(10)	79.88(8) – 123.15(8)
(M=Cs)	<2.957>		<107.27>	<98.90>
4.8	2.562(2) – 2.893(1)	2.639(1) – 2.929(1)	78.47(4) – 174.37(4)	79.63(4) – 167.37(4)
(M=K)	<2.684>	<2.790>	<102.75>	<98.07>
4.9	2.700(4) – 3.355(7)	2.777(5) – 3.197(5)	70.8(1) – 176.1(2)	65.7(1) – 176.5(1)
(M=Rb)	<2.838>	<2.945>	<98.7>	<97.9>
4.10	2.523(2) – 2.872(2)	2.669(2) – 2.687(2)	86.56(5) – 173.54(7)	85.92(2) – 151.09(6)
(M=K)	<2.642>	<2.678>	<108.70>	<104.55>

Considering the molecular structures of the lithium (**3.1**), sodium (**4.1**), potassium (**4.3**), and rubidium (**4.5**) analogues its rather amazing that all four complexes form molecular dimers. The aggregates are also retained when changing *para*-substituent (bromo and chloro). In our group's previously published lithium and sodium aryloxide systems, small changes to the system altered either the size of the aggregate or topology of the extended structure.[1] The major change between the complexes presented here is the increased dioxane solvation as the metal size increases. In turn, this effects the topology of the extended structures. However, the potassium and rubidium analogues are essentially identical in solvation and extended structure.

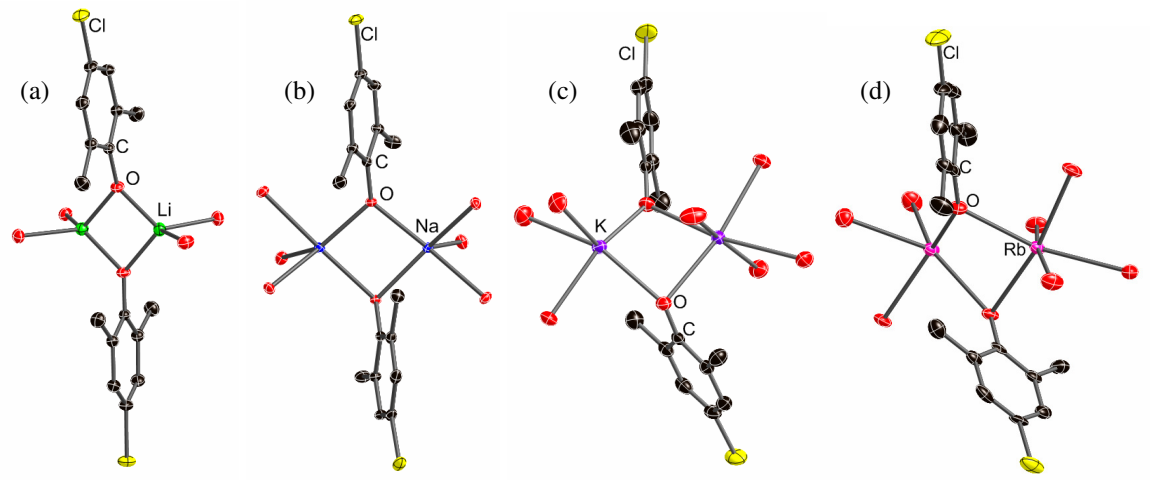

Figure 4.6 Complete series of dimeric alkali metal 4-Cl-2,6-dimethylphenoxide coordinated by (a) four dioxanes in **3.1**, (b) six dioxane in **4.1**, (c) seven dioxanes in **4.3**, and (d) seven dioxanes in **4.5**. Only the coordinating oxygen of the dioxane molecules are shown for clarity.

One interesting distinction in the series is the increased distortion of the M_2O_2 dimeric ring going from the lithium (**3.1**) to the rubidium (**4.5**) analogue. The four atoms that make up the M_2O_2 ring in **3.1** are essentially planar, with the largest distance from the mean plane being 0.020 Å. The atoms in the dimeric ring begin to distort from the

mean plane in **4.1** (0.046 - 0.077 Å), and then distort even further in **4.3** (0.275-0.209 Å) and **4.5** (0.294-0.341 Å). The best justification for this large distortion is that the larger metals allow for more movement of the aryloxides in order to pack the extended structure more efficiently.

4.3.3 Extended Structures

Although discussed first, the extended structure of **4.1** (and the isostructural **4.2**) is the hardest to describe and visually represent. Each of the dimeric sodium aggregates are coordinated by six dioxanes (Figure 4.7a). Four of the dioxanes bridge to four unique neighboring aggregates, while the remaining two dioxanes form a double-bridge to one neighboring aggregate, as shown in Figure 4.7b. The formation of double, and even triple, bridges between two aggregates has been seen before in other network structures.[9] In terms of topology, a double (or triple) bridge is isostructural to a single bridge. Therefore, each dimeric aggregate in **4.1** can be considered a five-connected node. The Schläfli symbol of the extended structure is $5^9.7$ (td10=2103) and the three-letter code in the RCSR database is **gan**. Although there have been previously synthesized 5-connected nets, the $5^9.7$ topology of **4.1** is completely novel.[10] A recent survey of the CSD showed that only 7.7 % of the characterized extended networks are constructed from pentagonal SBUs and nearly all of these have the closely related $4^4.6^6$ or $4^6.6^4$ topology.[6]

The network cannot be shown as a simpler series of intersecting subnets like the rest of the structures in this chapter because of its complicated structure. This is highlighted by Figure 4.7c, which shows one of the dimeric aggregates (shown in red) and the five labeled neighboring aggregates. Because each aggregate is 5-connected, there are 10 unique rings created. The Schläfli symbol of the extended structure is $5^9.7$,

which indicates that there are nine 5-membered rings and one 7-membered ring at each node. All ten rings are shown in Figure 4.7c, with the one 7-membered ring created from the angle between neighboring dimers 1 and 4. The angles between the rest of the neighboring dimers create the nine 5-membered rings.

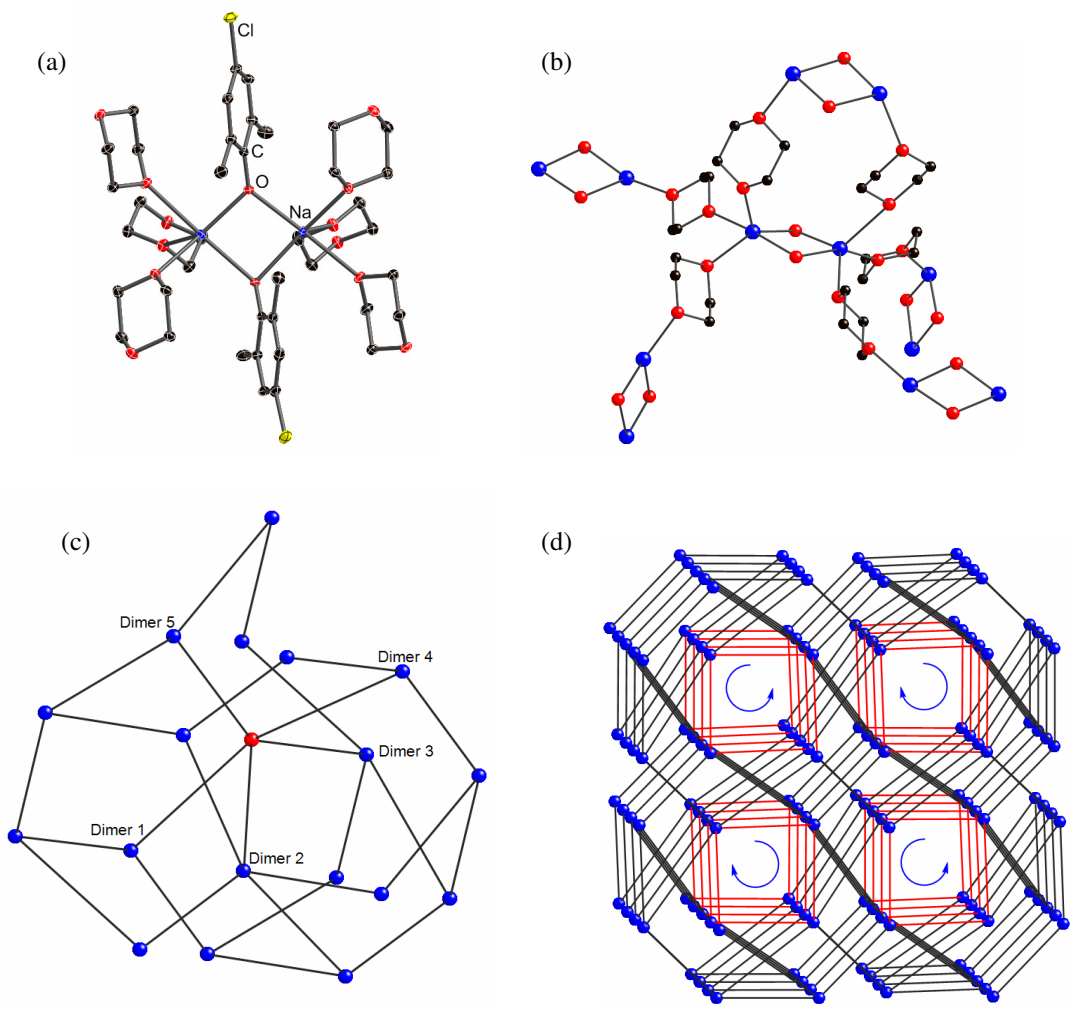

Figure 4.7 Structure of **4.1** showing (a) the dimeric aggregate with six coordinated dioxane molecules, (b) the dimeric aggregate bridged to five other aggregates through four single bridges and one double bridge, (c) the dimeric aggregate, shown in red, with the nine 5-membered rings and one 7-membered ring created by the coordination to five neighboring aggregates, and (d) extended 5^9.7-net with helical channels shown in red.

If the structure of **4.1** is expanded, as shown in Figure 4.7d, it can be seen that the network cannot be broken down into simpler subnets. One interesting feature of the extended structure is the formation of helical channels. These are shown in red in Figure 4.7d. Each helical channel has either a left- or right-handedness, but the overall net is not chiral because there are equal number of each channel in the overall structure. The synthesis of extended networks that have channels of only one-handedness are of interest to material scientists interstested in chiral separation. The network in **4.1** is not porous, however, because the sterically bulky aryloxide groups pack in the channels to remove most of the free space.

The extended structures of **4.3**-**4.6** are topologically equivalent so only **4.3** will be discussed. In the extended structure of **4.3** each dioxane acts as a divergent bridging ligand, so that each dimer connects to seven neighbors *i.e.* the dimers are septahedral nodes (Figure 4.8). Due to the complex nature of visualizing high-connectivity nets, **4.3** is most easily described in terms of interconnected simpler subnets. In these terms the extended can be described as parallel 4^4-nets that are intersected perpendicularly by a series of 6^3-nets (Figure 4.8d), *i.e.* four of the seven dioxane molecules connect to other dimers "in-plane" to give a two-dimensional 4^4-net, and the remaining three dioxane molecules bridge to identical 4^4-nets above or below this plane. Each vertex in the 4^4-net bridges to two vertices above and one vertex below (or vice-versa). The Schläfli symbol for the underlying topology of the 7-connected net is $3^3.4^{12}.5^5.6$ (td10 = 2198), which is an unprecedented topology for a coordination network.[5] This network is identified by the code **vcn** in the Reticular Chemistry Structure Resource (RCSR) database.[11] Although the extended structure has been theoretically predicted, and thus an entry in the RCSR

database, to the best of our knowledge this is a completely novel topology for an experimentally synthesized extended material.

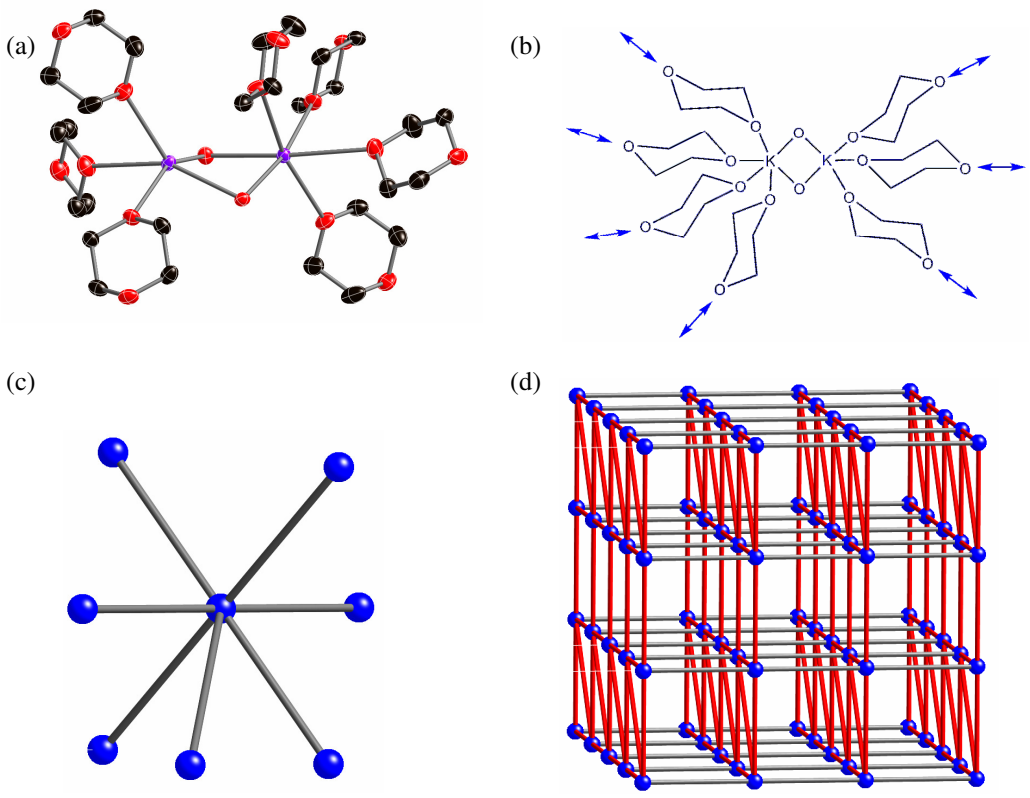

Figure 4.8 Structure of **4.3** showing (a) the dimeric aggregate coordinated by seven dioxanes with the carbon atoms of the aryloxide removed for clarity, (b) illustration of the dimeric aggregate with 7 points of extension, (c) the dimeric aggregate represented as a blue node connected to seven other aggregates, (d) the extended 7-connected network with $3^3.4^{12}.5^5.6$ topology.

High quality crystals of the cesium analogue of 4-Cl-2,6-dimethylphenoxide, $[(4\text{-Cl-2,6-Me}_2\text{-C}_6\text{H}_2\text{OCs})_7\cdot(\text{dioxane})_1]_\infty$ (**4.7**), was grown from a dioxane and toluene solution. Unlike every other compound crystallized from dioxane in our studies, the cesium aryloxide complex is not solvated by dioxane. The extended inorganic structure is built through only Cs-O_{Ar} interactions as well as Cs-C_{Ar} cation-π interactions. It is unsurprising that the structure is not coordinated by dioxane because there is always a

delicate balance between M-O_{Ar} and M-O_{Diox} interactions in solution. For the lighter alkali metals, the structures were stabilized as a dimeric aggregate coordinated by a large number of dioxane solvent molecules. That balance becomes shifted however when moving to cesium, resulting in an extended structure that is better classified as an inorganic, rather than a coordination, network. The asymmetric unit of **4.7** is composed of seven unique cesium aryloxides as shown in Figure 4.9.

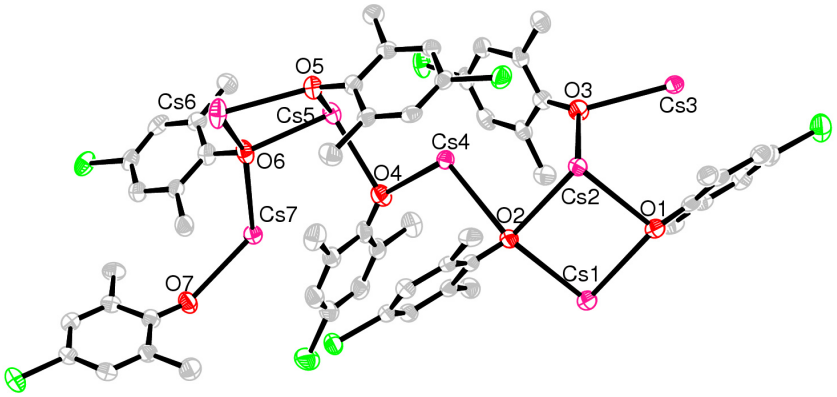

Figure 4.9 Asymmetric unit of **4.7** with seven unique cesiums and aryloxides. There is one free molecule of dioxane (not shown) per asymmetric unit in the channel of the extended structure.

There are three different cesium bonding environments in the structure (Figure 4.10). The first group (Cs1, Cs2, Cs5) each coordinate to two μ_3-aryloxide anions and one μ_2-aryloxide anion. The second group (Cs3, Cs4, Cs7) each coordinate to one μ_3-aryloxide anion and one μ_2-aryloxide anion. This group also coordinates to three different aryloxide rings through Cs-C_{Ar} cation-π interactions. The final cesium, Cs6, coordinates to two μ_3-aryloxide anions as well as three different aryloxide rings through Cs-C_{Ar} cation-π interactions. This last interaction with Cs6 is important to the overall structure and will be highlighted shortly. The other cation-π interactions do not change the

topology of the extended structure, but help fill the bonding environment of the cesiums. The Cs-C_{Ar} cation-π interactions range between 3.256(4) – 3.603(4) Å, which is only slightly longer than the Cs-O_{Ar} distances of 2.781(3) – 3.401(3).

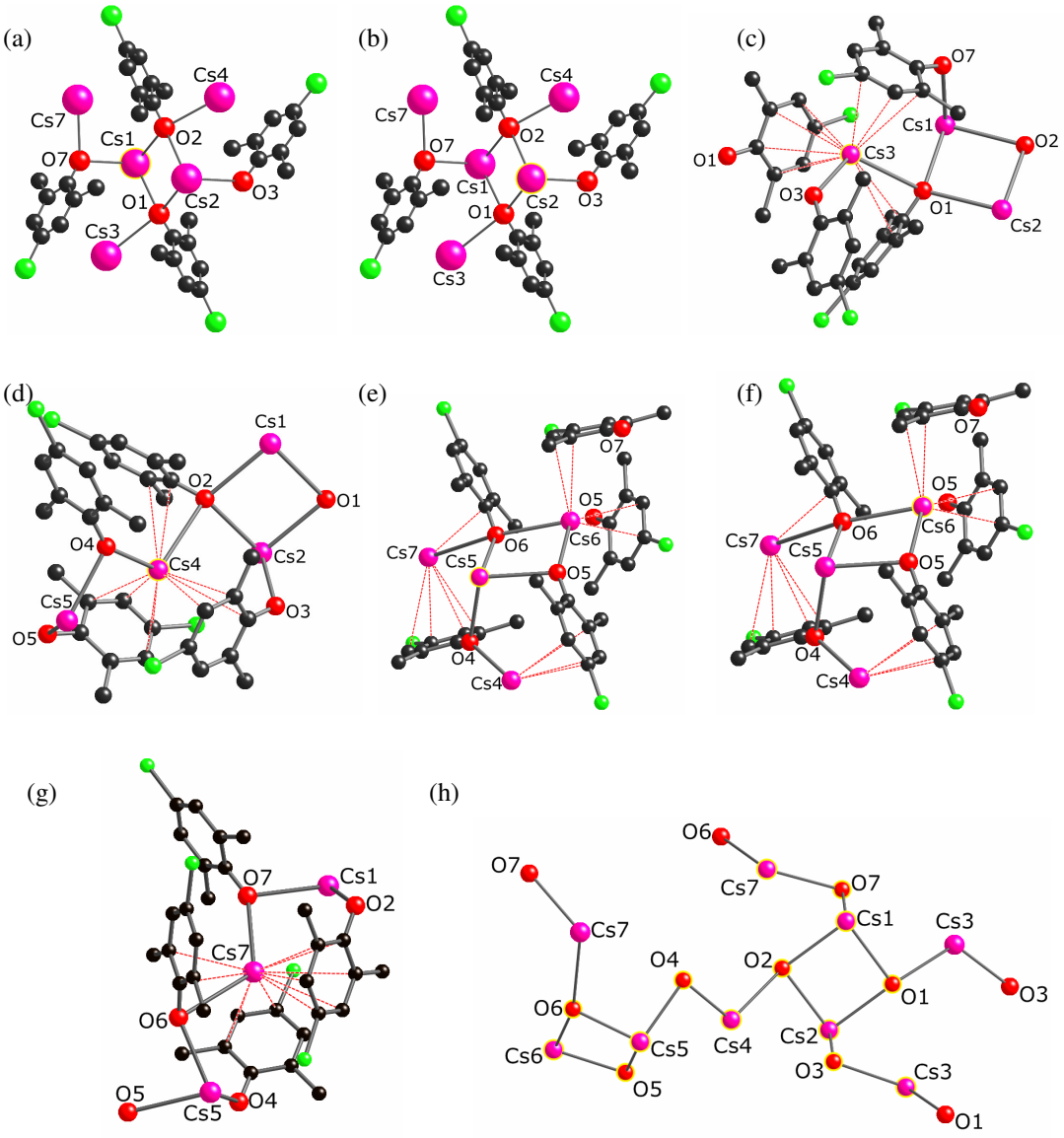

Figure 4.10 (a-g) Bonding environments of the seven cesium atoms in **4.7**. (h) Asymmetric unit (highlighted in yellow) with all points of extension through Cs-OAr interactions. Carbon atoms of the aryloxide backbones are removed for clarity.

The extended structure is built through the Cs-O_{Ar} interactions. The basic repeating unit is a 24 membered cesium aryloxide ring (Figure 4.11a). Each ring is composed of 4 Cs1-O1-Cs2-O2 dimers as well as 2 Cs5-O5-Cs6-O6 dimers. The six dimers are connected through the remaining Cs-O interactions. The 24 membered ring is connected to other rings through only the Cs1-Cs2 dimer (Figure 4.11b). Each Cs1-Cs2 dimer is part of four different rings.

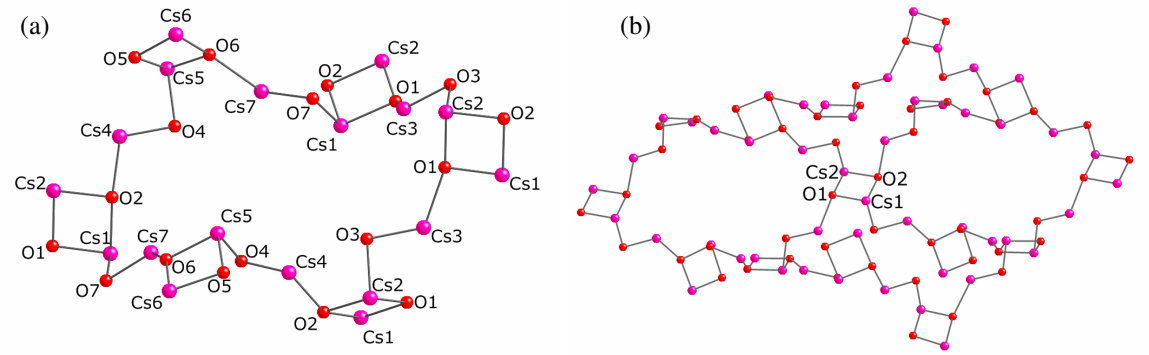

Figure 4.11 (a) Twenty-four membered ring building unit of **4.7** built through Cs-O interactions. (b) Four 24-membered rings connected through a Cs1-Cs2 dimer.

Expansion of the extended structure of **4.7** gives the one-dimensional tube structure seen in Figure 4.12. When only the Cs-O_{Ar} interactions are considered, the tube takes on a star structure with the Cs5-C6 dimer taking on the points of the star. The inner channel of the tube is porous with one disordered molecule of free dioxane present per asymmetric unit. The presence of free dioxane is further indication that the M-O_{Ar} is highly favored in this structure over M-O_{diox} interactions. The tubes are held together in the solid state through only the Cs6-C_{Ar} cation-π interactions mentioned earlier. Each tube is surrounded by six different tubes to give a hexagonal packing arrangement. With

this wholly unique structure, we are unaware of any other extended structure that has the same topology.

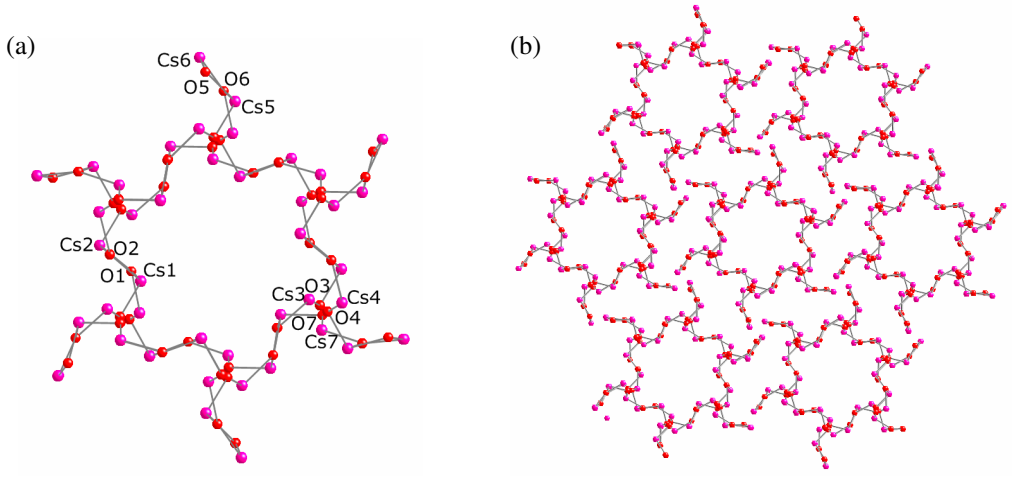

Figure 4.12 (a) Extended star-shaped tube structure of **4.7** built through cesium aryloxide interactions. (b) Packing of the one-dimensional tubes stabilized through cation-π interactions.

4.4 Reactions of 2,4,6-Trimethylphenol

4.4.1 Synthesis

The equimolar reaction of 2,4,6-trimethylphenol with KHMDS or RbHMDS in 1,4-dioxane resulted in the instant formation of a precipitate, which dissolved on vigorous heating. High-quality crystals of $[(2,4,6\text{-}Me_3\text{-}C_6H_2OM)_2\cdot(diox)_5]_\infty$, where M = K (**4.8**) or M = Rb (**4.9**) were grown from the dioxane reaction solution after individually optimizing their concentrations and temperatures for crystal growth. Subsequent equimolar reactions of 2,4,6-trimethylphenol with KHMDS in THF led to the formation of crystals of the THF solvate $[(2,4,6\text{-}Me_3\text{-}C_6H_2OK)_4\cdot(thf)_4]_\infty$ (**4.10**).

4.4.1 Molecular Structures

With the success of using 4-Cl/Br-2,6-dimethylphenoxide aggregates to construct high-connectivity networks, we wished to use the same synthetic approach to target related networks by modifying the substituents on the aryloxide anion. Replacement of the chloride at the *para*-position with a methyl substituent led to the unexpected formation of the pentameric aggregates $[(2,4,6\text{-}Me_3\text{-}C_6H_2OM)_2{\cdot}(diox)_5]_\infty$, where M = K (**4.8**) or M = Rb (**4.9**), as determined by single crystal X-ray diffraction.

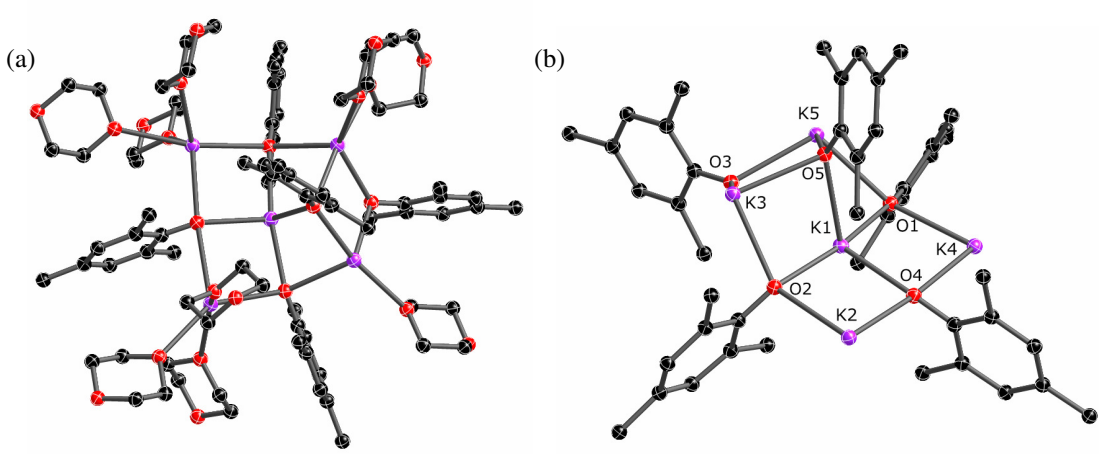

Figure 4.13 Structure of **4.8** showing (a) the full pentameric aggregate with nine coordinated dioxane molecules, and (b) the pentameric aggregate with dioxane molecules removed for clarity.

The molecular structure of **4.8** consists of a pentameric potassium aggregate where each of the potassium metals and aryloxide anions are in different bonding environments (Figure 4.13). K1 coordinates to four μ_3-aryloxide anions and is not solvated by dioxane. K2 coordinates to two μ_3-aryloxide anions and is solvated by three dioxane molecules, all of which bridge to other aggregates. K3 coordinates to two μ_3-aryloxide anions, and one μ_2-aryloxide anion. It is also solvated by two dioxane molecules, both which bridge to other aggregates. K4 coordinates to two μ_3-aryloxide

anions and is solvated by three dioxane molecules, where one is terminal and the second two bridge to other aggregates. K5 coordinates to two μ_3-aryloxide anions, and one μ_2-aryloxide anion. It is also solvated by one dioxane, which bridges to another aggregate. Because of the bonding, the pentameric aggregate could be described as a eight-membered K_4O_4 tetrameric ring with a potassium aryloxide at its center. The inner K-$O_{(Ar)}$ bond distances range between 2.562(1)-2.717(1) Å with a mean of 2.613 Å whereas the outer K-$O_{(Ar)}$ bond distances range between 2.626(1)-2.893(1) Å with a mean of 2.713 Å. The K-$O_{(diox)}$ distances are very similar to **4.1** with a range of 2.639(1) – 2.929(1) Å and a mean of 2.790 Å.

To date, there have only been four reports of homometallic alkali metal pentamers, all of which are lithium salts.[12] Indeed, pentameric aggregates of any metal are rare, with **4.8** having a unique structural core.[13] Figure 4.14a shows an illustration of the core aggregate of compound **4.8**, with the dioxanes and carbons of the aryloxides removed for clarity. Figure 4.14b-j shows all of the known structurally similar pentameric aggregates.[13] One way of deconstructing the pentameric aggregates is by the total number of metal-anion dimers. For example, the pentameric aggregate of **4.8** is composed of five dimers. In contrast, the pentameric aggregates shown in Figure 4.14b-j are composed of either four, six, eight, or twelve dimers. Although still rare, the pentameric aggregate with all of its structural variations is clearly an emerging aggregate type worthy of further study.

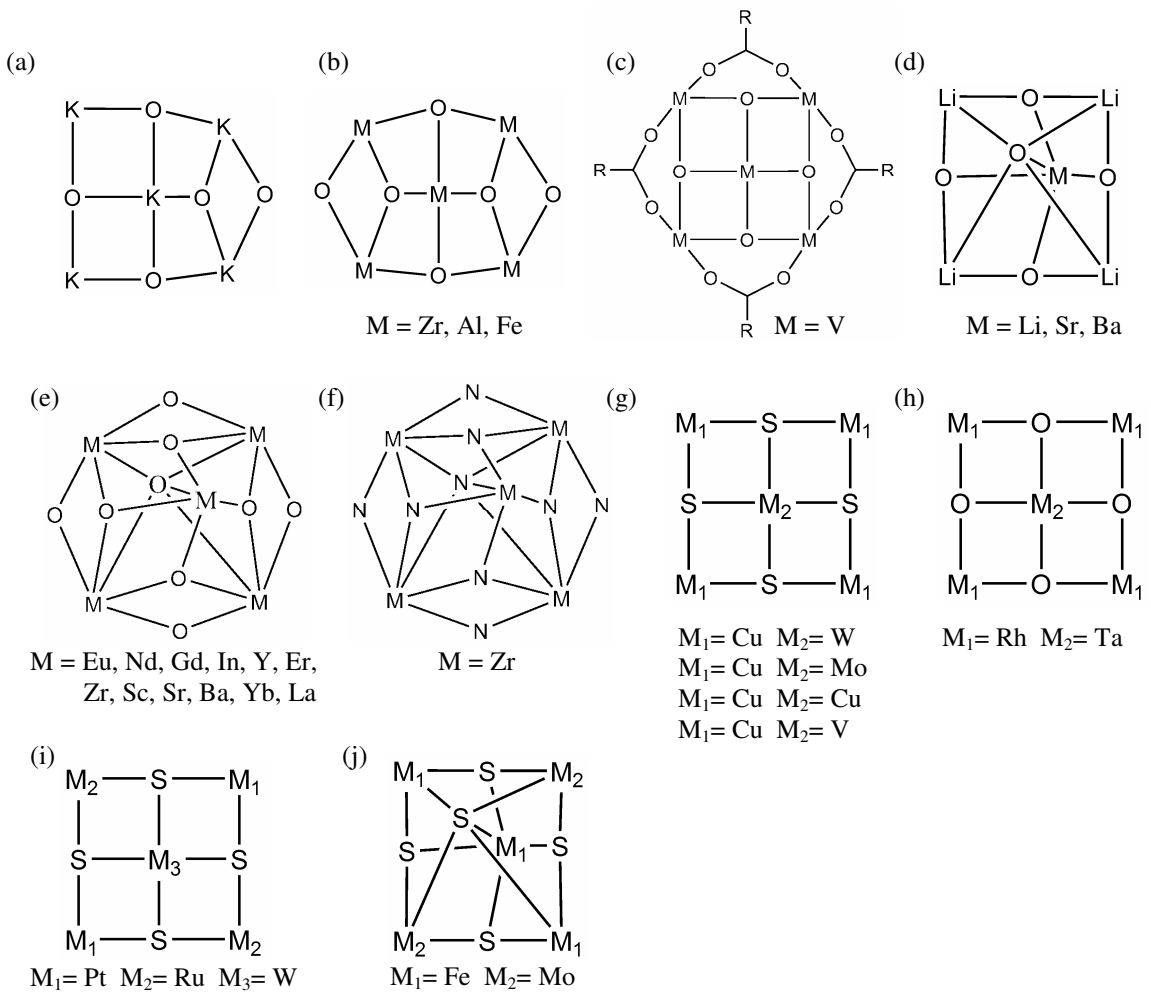

Figure 4.14 (a) Pentameric aggregate of **4.8**, and (b-j) core structures of related pentameric aggregates.

The pentameric aggregate of the rubidium analogue, **4.9**, is isostructural to **4.8** except for the number of coordinated dioxane molecules. The aggregate can again be described as an eight-membered Rb_4O_4 ring with an additional rubidium aryloxide at the core (Figure 4.15). Similar to **4.8**, the inner Rb-$O_{(Ar)}$ bond distances range between 2.700(4)-2.862(4) Å, with a mean of 2.768 Å, whereas the outer Rb-$O_{(Ar)}$ bond distances are longer with a range of 2.726(5)-3.355(7) Å and a mean of 2.838 Å. Two of the rubidium atoms along the outer ring are each coordinated by two dioxane molecules, with

the other two rubidium atoms coordinated by three dioxane molecules each to give a total of ten dioxanes solvating the aggregate. The Rb-$O_{(diox)}$ bond distances range between 2.777(5)-3.197(5) Å, with a mean of 2.945 Å.

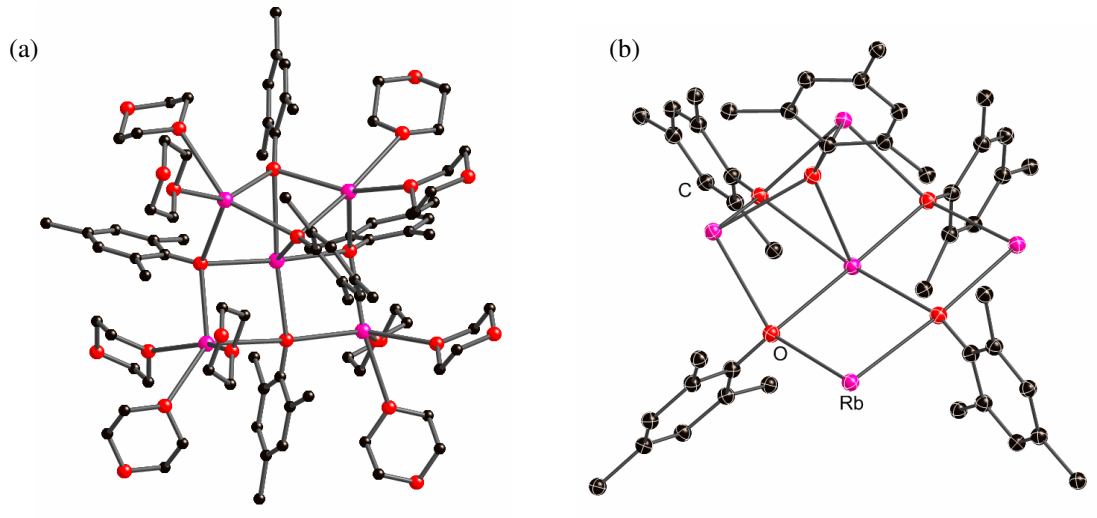

Figure 4.15 Structure of **4.9** showing (a) the full pentameric aggregate with ten coordinated dioxane molecules, and (b) the pentameric aggregate with dioxane molecules removed for clarity.

Due to the formation of the unique pentameric aggregates in **4.8** and **4.9**, the THF solvate of **4.8** was synthesized to determine if the structure would be retained. The solvate, $[(2,4,6\text{-}Me_3\text{-}C_6H_2OK)_4\cdot(thf)_4]_\infty$ (**4.10**), does not form the targeted pentameric aggregate, but instead forms a tetrameric ladder aggregate (Figure 4.16). Although not as common as tetrameric cubane aggregates, there are a number of tetrameric ladder aggregates in the CSD for alkali metal aggregates.[14]

Although the intended pentameric structure was not formed, the structure of **4.10** is interesting in its own right. The two potassiums at the ends of the tetrameric aggregate are η^6-coordinated to the aryloxide ring of a neighboring aggregate with K-C_{Ar} distances of 3.090 – 3.339 Å. This gives a one-dimensional chain polymer built up through cation-

π interactions. Of the few previously synthesized potassium aryloxide structures, only a couple form extended structures through K-C_{Ar} cation-π interactions.[2]

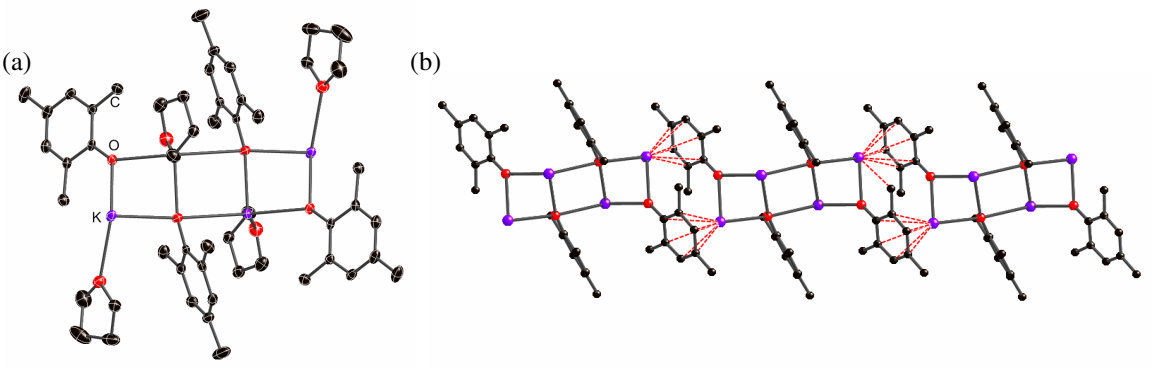

Figure 4.16 (a) Tetrameric ladder structure of **4.10** which is coordinated by four THF molecules. (b) Extended 1D structure built through cation-π interactions.

4.4.1 Extended Structures

Since the pentameric aggregate of **4.8** is relatively flat and open, it allows for coordination by a large number of solvent molecules. Two of the outer potassium atoms of the aggregate (K2 and K4) coordinate to three dioxanes, while the remaining two metals coordinate to either one (K5) or two (K3) dioxane (Figure 4.17). The interior metal is bonded to only the four of the aryloxide anions. This gives a total of nine coordinated dioxane molecules per pentamer. Six of the dioxane molecules form single bridges to six neighboring pentameric aggregates, two dioxanes form a double bridge to a single neighboring aggregate, and the final dioxane terminally solvates the aggregate. As mentioned earlier, the formation of a double bridge to a single aggregate was also seen in **4.1** and in other high-connectivity networks. In topological terms, the pentameric aggregate in **4.8** acts as a 7-connected node to give an extended network of parallel 4^4-nets that are perpendicularly intersected by parallel 6^3-nets (Figure 4.16d). The 3D

structure adopts a $4^{15}.6^6$ topology (td10=2206), which is not only an unprecedented topology for coordination networks, but is not even a theoretical structure in the RCSR or EPINET databases.[5]

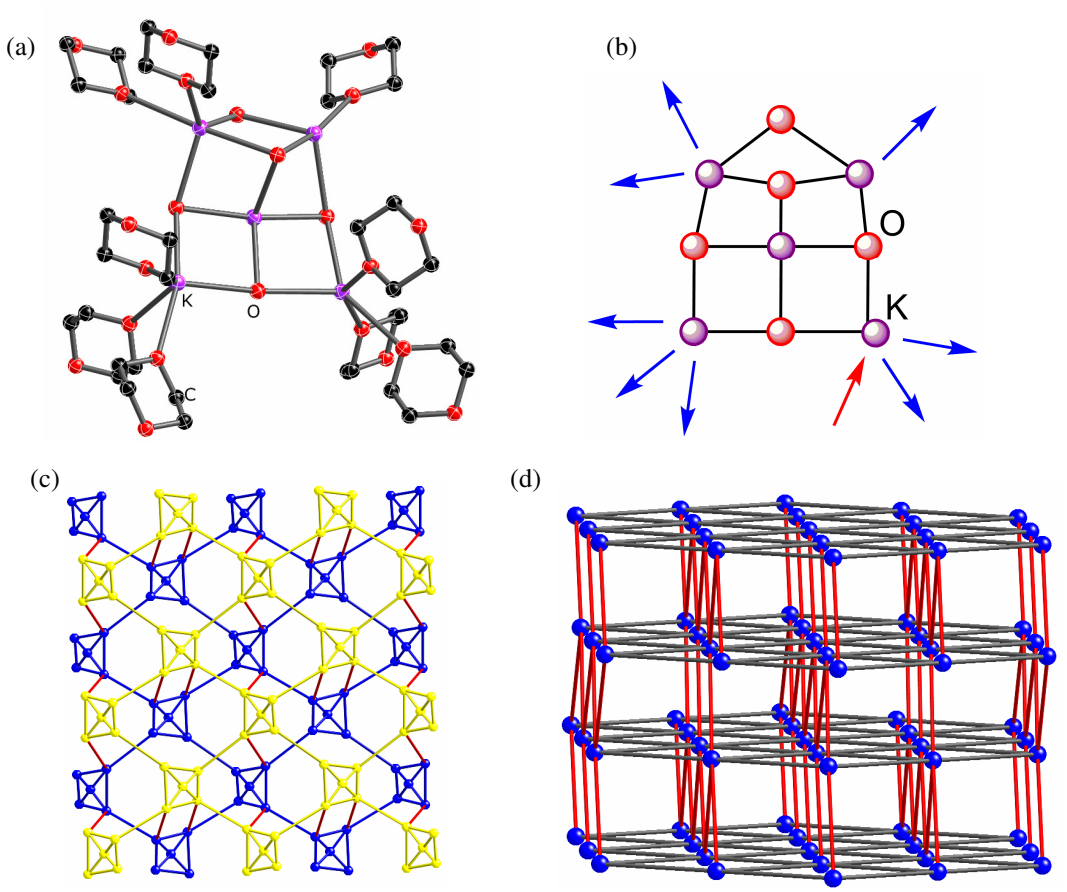

Figure 4.17 Structure of **4.8** showing (a) the pentameric aggregate coordinated by nine dioxanes, (b) an illustration of the aggregate showing eight bridging and one terminal dioxane, (c) two 4^4-net layers of the extended structure showing the top layer (yellow) connected to the bottom layer (blue) through a combination of single and double dioxane bridges, (d) the extended structure with pentameric aggregates shown as blue spheres.

Of note here is the only other example of a uninodal 7-connected network, namely $\{[La(L)_4](BPh_4)(ClO4)_3 \cdot 2.75MeOH\}_\infty$, L = 4,4′-bipyridine-N,N′-dioxide, **4.13**.[15] This network, identified by the code **sev** in the RCSR database,[5] is constructed from single

La(III) metal centers that are coordinated by eight bridging 4,4′-bipyridine-N,N′-dioxides. Six of the linkers form single bridges to six neighboring metals, while the remaining two form a double bridge to a single metal center. Each of the metals therefore act as a 7-connected node as shown in Figure 4.18b, to give a network with the Schläfli symbol of $4^{17}.6^4$.

The variance between the topologies of the previously discussed 7-connected network, **4.3**, and that of **4.13** is highlighted by their different Schläfli symbols, and can be seen illustratively in Figures 4.18a and 4.18b. In the extended structures of **4.3** the 6^3-subnets are aligned along the ring edges of the 4^4-nets. In comparison, the 6^3-subnets in **4.13** traverse the face of the aligned 4^4-nets. This topological difference is comparable to that between the 6-connected **pcu** and 8-connected **bcu** nets. The **pcu** and **bcu** networks can be simplified into parallel sheets of 4^4-subnets that are perpendicularly intersected by a similar series of 4^4-subnets. However, in the **pcu** net the perpendicular subnets intersect along the ring edges, whereas in the **bcu** net the subnets intersect across the face of the ring.

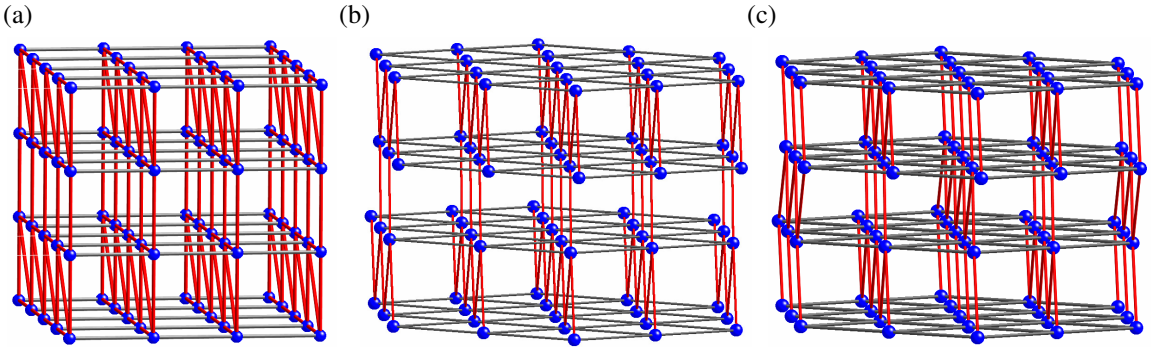

Figure 4.18 Extended structures of the three known 7-connected topologies showing (a) **4.3**, (b) **4.13**, and (c) **4.8**.

The gross topologies of **4.13** and **4.8** are quite similar (Figure 4.18b,c). The Schläfli symbol of $4^{17}.6^4$ for **4.13** and $4^{15}.6^6$ for **4.8** indicates that only two of the rings formed at each node differ in size. In both structures, the 6^3-nets perpendicularly intersect the 4^4-nets across the ring face. In **4.13**, the 6^3-nets are perfectly eclipsed, beginning and ending at the same 4^4-net layer. However, in **4.8** alternate 6^3-nets are offset from each other, beginning and ending at different 4^4-net layers. The staggered pattern of the 6^3-nets in **4.8** leads to the novel $4^{15}.6^6$ topology.

The pentameric aggregate of **4.9** is coordinated by ten dioxane molecules (Figure 4.19). Unlike **4.8**, all of the dioxanes bridge to other aggregates. Six of the of the dioxane molecules form single bridges to six neighboring pentameric aggregates, while the remaining four dioxanes form two double bridges to two neighboring aggregates. Because of the two double bridges each pentameric aggregate in **4.9** acts as an 8-connected node. The extended structure adopts the high-symmetry body-centered cubic net, which has a $4^{24}.6^4$ topology. Although still rare, there have been a number of recent reports of coordination networks adopting the **bcu** topology.[8] The three-dimensional structure can best be described in terms of simpler interconnected subnets. As shown in Figure 4.19d, the extended **bcu** topology can be shown as a parallel series of 4^4- nets (shown in red) that are intersected perpendicularly by another series of 4^4-nets (shown in gray).

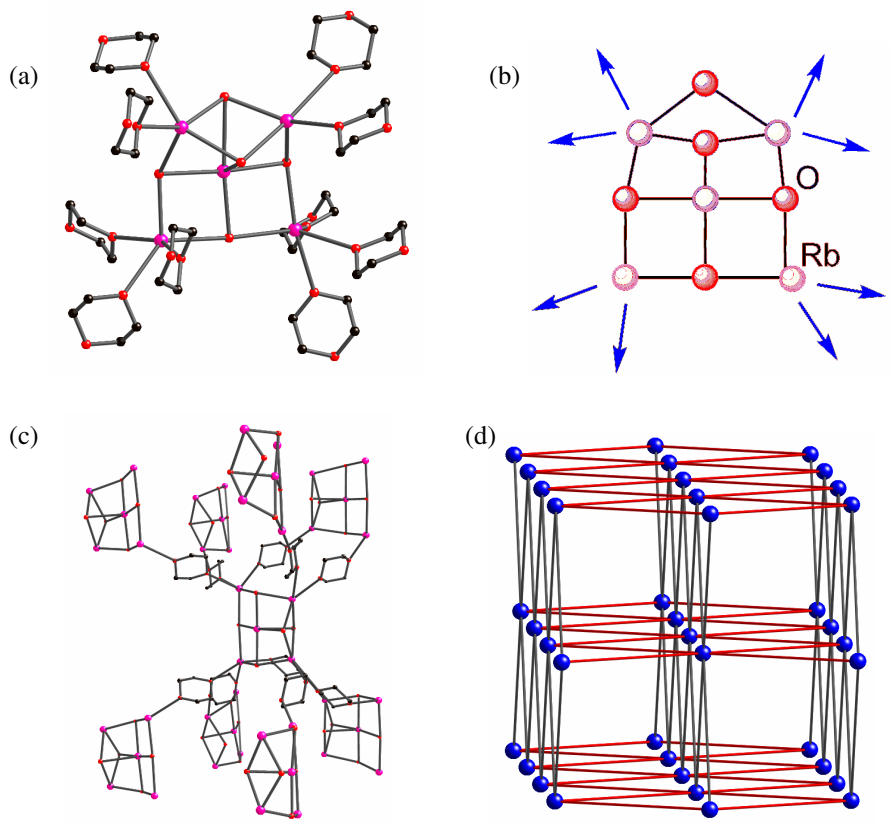

Figure 4.19 Structure of **4.9** showing (a) the pentameric aggregate coordinated by 10 dioxanes, (b) an illustration of aggregate showing eight unique points of extension, (c) the pentameric aggregate bridged through dioxane to eight neighboring aggregates, (d) the extended structure with **bcu** topology.

4.5 Summary

The characterization of the 2,4,6-trisubstitutued aryloxide aggregates, **4.1**-**4.10**, demonstrate that both dimeric and pentameric nodes can be used as SBUs in the synthesis of extended coordination networks. Furthermore, both types of nodes allow for highly solvated systems, which has led to the formation of completely novel topologies for the extended materials.

An interesting aspect of 7-connected networks is that unlike 4-, 6-, 8- and 12-connected nets there is no highest symmetry topology. Surprisingly, three distinct

topologies of 7-connected nets have been discovered from the five 7-connected network presented here and the one previously characterized.[15] Also, the new topology reported here for **4.8** is not even predicted in the RCSR database. Systematic synthesis and classification is beginning to show underlying structural patterns however. For example, all three 7-connected nets can be deconstructed into simpler 4^4- and 6^3-subnets. Further work from our group and others will help shed light on the generality of these unique topologies.

4.6 Experimental Section

4.6.1 General Procedures

All experimental manipulations were performed under a dry nitrogen atmosphere using standard Schlenk techniques, or in an argon-filled glovebox.[16] All glassware was flame-dried under vacuum before use. Hexane was dried immediately before use by passage through columns of copper-based catalyst and alumina (Innovative Technology), and stored over 4 Å molecular sieves. Dioxane was purchased from Acros and was distilled over sodium benzophenone under N_2 prior to use. The phenols were purchased from Aldrich and were recrystallized from hexane. KHMDS was purchased from Aldrich and was used as received. $[RbOBu^t \cdot Bu^tOH]_\infty$, RbHMDS, and CsHMDS were prepared by literature methods.[17,18] Deuterated solvents were purchased from Cambridge Isotope Laboratories and were dried by storage over 4 Å molecular sieves. ^1H and ^{13}C NMR spectra were recorded on either a Varian Unity Plus 300 MHz or a Bruker AVANCE

DPX-400 spectrometer at 293 K, and were referenced internally to the residual signals of the deuterated solvents.

4.6.2 X-ray Crystallography

Crystals were examined under Infineum V8512 oil. The datum crystal was affixed to a thin glass fibre mounted atop a tapered copper mounting-pin and transferred to the 100 K nitrogen stream of a Bruker APEX II diffractometer equipped with an Oxford Cryosystems 700 series low-temperature apparatus. Cell parameters were determined using reflections harvested from three sets of 20 0.3° ω scans. The orientation matrix derived from this was passed to COSMO to determine the optimum data collection strategy.[19] Cell parameters were refined using reflections with $I \geq 10\sigma(I)$ harvested from the entire data collection. All data were corrected for Lorentz and polarization effects, as well as for absorption. Tables A.4, A.5, and A.6 list the key crystallographic parameters for **4.1**-**4.10**. The structures were solved and refined using SHELXTL.[20] Structure solution was by direct methods. Non-hydrogen atoms not present in the direct methods solution were located by successive cycles of full-matrix least-squares refinement on F^2. All non-hydrogen atoms were refined with parameters for anisotropic thermal motion. Hydrogen atoms were placed at idealized geometries and allowed to ride on the position of the parent atom. Hydrogen thermal parameters were set to 1.2× the equivalent isotropic U of the parent atom, 1.5× for methyl hydrogens.

4.6.3 Preparation and Characterization

4.1 $[(4\text{-Cl-}2,6\text{-Me}_2\text{-C}_6\text{H}_2\text{ONa})_2\cdot(\text{dioxane})_3]_\infty$ - NaH (5 mmol, 120 mg) was added to a stirred solution of 4-Cl-2,6-dimethylphenol (5 mmol, 783 mg) in dioxane (20 mL). A

white precipitate formed, which completely dissolved on heating the solution to reflux. X-ray quality crystals were obtained by slowly cooling the resulting solution in a hot water bath. Crystalline yield: 627 mg, 35.3%. δ_H (d_6-DMSO, 293K): 1.91 (s, 12H, *o*-Me), 3.57 (s, 24H, CH_2, dioxane), 6.61 (s, 4H, *m*-H). δ_c (d_6-DMSO, 293K) 18.19 (*o*-Me), 66.37 (CH_2, dioxane), 125.05 (*o*-C, Ph), 128.98 (*m*-C, Ph).

4.2 $[(4\text{-Br-}2,6\text{-}Me_2\text{-}C_6H_2ONa)_2\cdot(dioxane)_3]_\infty$ - NaH (5 mmol, 120 mg) was added to a stirred solution of 4-Br-2,6-dimethylphenol (5 mmol, 1005 mg) in dioxane (20 mL). A white precipitate formed, which completely dissolved on heating the solution to reflux. X-ray quality crystals were obtained by slowly cooling the resulting solution in a hot water bath. Crystalline yield: 881 mg, 56.8%. δ_H (d_6-DMSO, 293K): 1.90 (s, 12H, *o*-Me), 3.57 (s, 24H, CH_2, dioxane), 6.66 (s, 4H, *m*-H). δ_c (d_6-DMSO, 293K) 18.08 (*o*-Me), 66.37 (CH_2, dioxane), 126.10 (*o*-C, Ph), 128.72 (*m*-C, Ph).

4.3 $[(4\text{-Cl-}2,6\text{-}Me_2\text{-}C_6H_2OK)_2\cdot(dioxane)_{3.5}]_\infty$ - KHMDS (5 mmol, 997 mg) was added to a stirred solution of 4-Cl-2,6-dimethylphenol (5 mmol, 783 g) in dioxane (10 mL). A white precipitate formed, which completely dissolved on heating the solution to reflux. X-ray quality crystals were obtained by slowly cooling the resulting solution in a hot water bath. Crystalline yield: 582 mg, 33.4 %. δ_H (d_6-DMSO, 293K) 1.86 (s, 12H, *o*-Me), 3.57 (s, 28H, CH_2, dioxane), 6.50 (s, 4H, *m*-H). δ_c (d_6-DMSO, 293K) 18.31 (*o*-Me), 66.37 (CH_2, dioxane), 124.77 (*o*-C, Ph), 125.87 (*m*-C, Ph).

4.4 $[(4\text{-Br-}2,6\text{-}Me_2\text{-}C_6H_2OK)_2\cdot(dioxane)_{3.5}]_\infty$ - KHMDS (5 mmol, 997 mg) was added to a stirred solution of 4-Br-2,6-dimethylphenol (5 mmol, 1005 mg) in dioxane (20 mL). A white precipitate formed, which completely dissolved on heating the solution to reflux. X-ray quality crystals were obtained by slowly cooling the resulting solution in a

hot water bath. Crystalline yield: 405 mg, 20.6%. δ_H (d_6-DMSO, 293K) 1.86 (s, 12H, *o*-Me), 3.57 (s, 28H, CH_2, dioxane), 6.61 (s, 4H, *m*-H). δ_c (d_6-DMSO, 293K) 18.23 (*o*-Me), 66.36 (CH_2, dioxane), 125.81 (*o*-C, Ph), 128.59 (*m*-C, Ph).

4.5 $[(4\text{-Cl-}2,6\text{-}Me_2\text{-}C_6H_2ORb)_2\cdot(dioxane)_{3.5}]_\infty$ - RbHMDS (1 mmol, 246 mg) was added to a stirred solution of 4-Cl-2,6-dimethylphenol (1 mmol, 157 mg) in dioxane (10 mL). A white precipitate formed, which completely dissolved on heating the solution to reflux. X-ray quality crystals were obtained by slowly cooling the resulting solution in a hot water bath. Crystalline yield: 260 mg, 65.8 %. δ_H (d_6-DMSO, 293K) 1.85 (s, 12H, *o*-Me), 3.57 (s, 28H, CH_2, dioxane), 6.50 (s, 4H, *m*-H). δ_c (d_6-DMSO, 293K) 66.34 (CH_2, dioxane).

4.6 $[(4\text{-Br-}2,6\text{-}Me_2\text{-}C_6H_2ORb)_2\cdot(dioxane)_{3.5}]_\infty$ - $[RbOBu^t\cdot Bu^tOH]_\infty$ (2 mmol, 460 mg) was added to a stirred solution of 4-Br-2,6-dimethylphenol (2 mmol, 402 mg) in dioxane (20 mL). A white precipitate formed, which completely dissolved on heating the solution to reflux. X-ray quality crystals were obtained by slowly cooling the resulting solution in a hot water bath. Crystalline yield: 410 mg, 46.6%. δ_H (d_6-DMSO, 293K) 1.83 (s, 12H, *o*-Me), 3.57 (s, 28H, CH_2, dioxane), 6.58 (s, 4H, *m*-H).

4.7 $[(4\text{-Cl-}2,6\text{-}Me_2\text{-}C_6H_2OCs)_7\cdot(dioxane)_1]_\infty$ - CsHMDS (2 mmol, 586 mg) was added to a stirred solution of 4-Cl-2,6-dimethylphenol (2 mmol, 314 mg) in dioxane (9.5 mL) and toluene (15 mL). A white precipitate formed, which completely dissolved on heating the solution to reflux. X-ray quality crystals were obtained by slowly cooling the resulting solution in a hot water bath. Crystalline yield: 105 mg, 18.2 %. δ_H (d_6-DMSO, 293K) 1.93 (s, 42H, *o*-Me), 3.57 (s, 8H, CH_2, dioxane), 6.59 (s, 14H, *m*-H).

4.8 [(2,4,6-Me$_3$-C$_6$H$_2$OK)$_5$·(dioxane)$_5$]$_\infty$ - KHMDS (3 mmol, 598 mg) was added to a stirred solution of 2,4,6-trimethylphenol (3 mmol, 409 mg) in dioxane (10 mL). A white precipitate formed, which completely dissolved on heating the solution to reflux. X-ray quality crystals were obtained by slowly cooling the resulting solution in a hot water bath. Crystalline yield: 173 mg, 33.3 %. δ_H (d_6-DMSO, 293K) 1.89 (s, 30H, *o*-Me), 1.99 (s, 15H, *p*-Me), 3.58 (s, 40H, CH_2, dioxane), 6.39 (s, 10H, *m*-H). δ_c (d_6-DMSO, 293K) 18.74 (*o*-Me), 20.61 (*p*-Me), 66.37 (CH_2, dioxane), 111.16 (*p*-C, Ph), 122.63 (*o*-C, Ph), 127.77 (*m*-C, Ph), 167.30 (*i*-C, Ph).

4.9 [(2,4,6-Me$_3$-C$_6$H$_2$ORb)$_5$·(dioxane)$_5$]$_\infty$ - RbHMDS (0.41 mmol, 101 mg) was added to a stirred solution of 2,4,6-trimethylphenol (0.41 mmol, 56 mg) in dioxane (4 mL) and hexane (5 mL). A white precipitate formed, which completely dissolved on heating the solution to reflux. X-ray quality crystals were obtained by slowly cooling the resulting solution in a hot water bath. Crystalline yield: 96 mg, 6.1 %. δ_H (d_6-DMSO, 293K) 1.86 (s, 30H, *o*-Me), 1.98 (s, 15H, *p*-Me), 3.56 (s, 40H, CH_2, dioxane), 6.36 (s, 10H, *m*-H).

4.10 [(2,4,6-Me$_3$-C$_6$H$_2$OK)$_4$·(thf)$_4$]$_\infty$ - KHMDS (3 mmol, 598 mg) was added to a stirred solution of 2,4,6-trimethylphenol (3 mmol, 409 mg) in THF (2 mL) and hexane (4 mL). X-ray quality crystals were obtained by cooling the light purple solution to -20 °C for 72 h. Crystalline yield: 173 mg, 33.3 %. δ_H (d_6-DMSO, 293K) 1.76 (s, 8H, thf), 1.91 (s, 24H, *o*-Me), 2.00 (s, 12H, *p*-Me), 3.61 (s, 8H, thf), 6.40 (s, 8H, *m*-H).

4.7 References

[1] (a) MacDougall, D. J.; Morris, J. J.; Noll, B. C.; Henderson, K. W. *Chem. Commun.* **2005**, 456. (b) MacDougall, D. J.; Noll, B. C.; Henderson, K. W. *Inorg. Chem*. **2005**, *44*, 1181. (c) Morris, J. J.; Noll, B. C.; Henderson, K. W. *Cryst. Growth Des.* **2006**, *6*, 1071. (d) Morris, J. J.; Noll, B. C.; Honeyman, G. G.; Kennedy, A. R.; Mulvey, R. E.; Henderson, K. W. *Chem. –Eur. J.* **2007**, *13*, 4418. (e) Morris, J. J.; Noll, B. C.; Henderson, K. W. *Chem. Commun.* **2007**, 5191. (f) Morris, J. J.; Noll, B. C.; Schultz, A. J.; Piccoli, P. M. B.; Henderson, K. W. *Inorg. Chem.* **2007**, *46*, 10473.

[2] (a) Boyle, T.J.; Andrews, N.L.; Rodriguez, M.A; Campana, C.; Yiu, T. *Inorg. Chem*. **2003**, *42*, 5357. (b) Arnold, P.L.; Hall, J.J.; Natrajan, L.S.; Blake, A.J.; Wilson, C.; *Daltan Trans*. **2003**, 1053. (c) Dinger, M.B.; Scott, M.J.; *Inorg Chem*. **2000**, *39*, 1238. (d) Dinnebier, R.E.; Pink, M.; Sieler, J.; Norby, P.; Stephans, P.W. Inorg. Chem. 1998, 37, 4996. (e) Cole, M. L.; Higham, L. T.; Junk P. C.; Proctor, K. M.; Scott, J. L.; Strauss, C. R. *Inorg. Chim. Acta* **2005**, *358*, 3159.

[3] (a) Harrowfield, J. M.; Skelton, B. W.; White, A. H. *Aust. J. Chem.* **1995**, *48*, 1311. (b) Dinnebier, R. E.; Pink, M.; Sieler, J.; Stephans, P. W.; *Inorg. Chem.* **1997**, *36*, 3398. (c) Harrowfield, J. M.; Sharma, R. P.; Skelton, B. W.; White, A. H. *Aust. J. Chem.* **1998**, *51*, 747. (d) Dinnebier, R. E.; Jelonek, S.; Sieler, J.; Stephans, P. W. *Z. Anorg. Allg. Chem.* **2002**, *628*, 363. (e) Couhorn, U.; Dronskowski, R. *Z. Anorg. Allg. Chem.* **2004**, *629*, 647. (f) Weinert, C. S.; Fanwick, P.; Rothwell, I. P. *Inorg. Chem.* **2003**, *42*, 6089. (g) Bunge, S. D.; Boyle, T. J.; Pratt III, H. D.; Alam, T. M.; Rodriguez, M. A. *Inorg. Chem.* **2004**, *43*, 6035. (h) Hu, M.; Geng, C.; Li, S.; Du, Y.; Jiang, Y.; Liu, Z. *J. Organomet. Chem.* **2005**, *690*, 3118. (i) Westerhausen, M.; Ossberger, M. W.; Alexander, J. S.; Ruhlandt-Senge, K. *Z. Anorg. Allg. Chem.* **2005**, *631*, 2836. (j) Pink, M.; Sieler, J. *Inorg. Chim. Acta* **2007**, *360*, 1221.

[4] Hyde, S. T.; Delgado-Friedrichs, O.; Ramsden, S. J.; Robins, V. *Solid State Sci.* **2006**, *8*, 740.

[5] (a) O'Keeffe, M.; Yaghi, O. M.; Ramsden, S. Reticular Chemistry Structure Resource, Arizona State University, Tempe, AZ, 2007, Database available at http://rcsr.anu.edu.au/; (b) Ramsden, S.; Robins, V.; Hyde, S. T.; Hungerford, S. EPINET: Euclidean patterns in non-Euclidean tilings, 2006, http://epinet.anu.edu.au; (c) V. A. Blatov, http://www.topos.ssu.samara.ru/, 2007.

[6] Ockwig, N. W.; Delgado-Friedrichs, O.; O'Keeffe, M.; Yaghi, O. M. *Acc. Chem. Res.* **2005**, *38*, 176.

[7] Delgado-Friedrichs, O.; O'Keeffe, M.; Yaghi, O. M. *Phys. Chem. Chem. Phys*., **2007**, *9*, 1035.

[8] (a) Long, D. -L.; Blake, A. J.; Champness, N. R.; Wilson, C.; Schröder, M. *Angew. Chem. Int. Ed.* **2001**, *40*, 2443. (b) Luo, T. –T.; Tsai, H. –L.; Yang, S. –L.; Liu, Y. –H.; Yadav, R. D.; Su, C. –C.; Ueng, C. –H.; Lin, L. –G.; Lu, K. –L. *Angew. Chem. Int. Ed.* **2005**, *44*, 6063. (c) Zhang, X. –M.; Fang R. –Q.; Wu, H. –S. *J. Am. Chem. Soc.* **2005**, *127*, 7670. (d) Li, D.; Wu, T.; Zhou, X. –P.; Zhou, R.; Huang, X. –C. *Angew. Chem. Int. Ed.* **2005**, *44*, 4175. (e) Fang, Q. –R.; Zhu, G. –S.; Jin, Z.; Xue, M.; Wei, X.; Wang, D. –J.; Qiu, S. –L. *Angew. Chem. Int. Ed.* **2006**, *45*, 6126. (f) Zhang, J.; Kang, Y.; Zhang, J.; Li, Z. –J.; Qin, Y. –Y.; Yao, Y. –G. *Eur. J. Inorg. Chem.* **2006**, 2253.

[9] (a) Pan, L.; Liu, H.; Lei, X.; Huang, X.; Olson, D. H.; Turro, N. J.; Li, J. *Angew. Chem. Int. Ed.* **2003**, *42*, 542. (b) Long, D. –L.; Hill, R. J.; Blake, A. J.; Champness, N. R.; Hubberstey, P.; Proserpio, D. M.; Wilson, C.; Schröder, M. *Angew. Chem. Int. Ed.* **2004**, *43*, 1851 (c) Wang, X. –L.; Qin, C.; Wang, E. –B.; Su, Z. –M.; Xu, L.; Batten, S. R. *Chem. Commun.* **2005**, 4789. (d) Wang, X. –L.; Qin, C.; Wang, E. –B.; Su, Z. –M. *Chem. Eur. J.* **2006**, *12*, 2680. (e) Jia, J.; Lin, X.; Wilson, C.; Blake, A. J.; Champness, N. R.; Hubberstey, P.; Walker, G.; Cussen, E. J.; Schröder, M.; *Chem. Commun.* **2007**, 840 (f) Qu, X.; Xu, L.; Gao, G.; Li, F.; Yang, Y. *Inorg. Chem.* **2007**, *46*, 4775.

[10] For recent examples: (a) Wu, L. P.; Yamagiwa, Y.; Kuroda-Sowa, T.; Kamikawa, T.; Munakata, M. *Inorg. Chim. Acta* **1997**, *256*, 155. (b) Vaid, T. P.; Lobkovsky, E. B.; Wolczanski, P. T. *J. Am. Chem. Soc.* **1997**, *119*, 8742 (c) Cai, H.; Hu, H.-M.; Chen, W.-Z.; Zhu, H.-G.; You, X.-Z. *Chem. Lett.* **1999**, 221. (d) Vaid, T. P.; Tanski, J. M.; Pette, J. M.; Lobkovsky, E. B.; Wolczanski, P. T. *Inorg. Chem.* **1999**, *38*, 3394. (e) Sun, B.-W.; Gao, S.; Ma, B.-Q.; Niu, D.-Z.; Wang, Z.-M. *J. Chem. Soc., Dalton Trans.* **2000**, 4187. (f) Trombe, J. C.; Romero, S. *Solid State Sci.* **2000**, *2*, 279. (g) Long, D. L.; Blake, A. J.; Champness, N. R.; Wilson, C.; Schröder, M. *J. Am. Chem. Soc.* **2001**, *123*, 3401. (h) Evans, O. R.; Lin, W. *Chem. Mater.* **2001**, *13*, 3009. (i) Cui, C.-P.; Dai, J.-C.; Du, W.-X.; Fu, Z.-Y.; Hu, S.-M.; Wu, L.-M.; Wu, X.-T. *Polyhedron* **2002**, *21*, 175. (j) Maji, T. K.; Sain, S.; Mostafa, G.; Lu, T.-H.; Ribas, J.; Monfort, M.; Chaudhuri, N. R. *Inorg. Chem.* **2003**, *42*, 709. (k) Zhang, X.; Lu, C.; Zhang, Q.; Lu, S.; Yang, W.; Liu, J.; Zhuang, H. *Eur. J. Inorg. Chem.* **2003**, 1181. (l) Papatriantafyllopoulou, C.; Raptopoulou, C. P.; Terzis, A.; Janssens, J. F.; Manessi-Zoupa, E.; Perlepes, S. P.; Plakatouras, J. C. *Polyhedron*, **2007**, *26*, 4053. (m) Du, M.; Li, C.-P.; Zhao, X.-J.; Yu, Q. *CrystEngComm* **2007**, *9*, 1011. (n) Kelly, N. R.; Goetz, S.; Batten, S. R.; Kruger, P. E. *CrystEngComm* **2008**, *10*, 68.

[11] Blatov, V. A. *Acta Crystallogr., Sect. A: Found. Crystallogr.* **2007**, *A63*, 329.

[12] (a) Beswick, M. A.; Elvidge, B. R.; Feeder, N.; Kidd, S. J.; Wright, D. S.; *Chem. Commun*. **2001**, 379. (b) Davidson, M. G.; Howard, J. A. K.; Lamb, S.; Lehmann, C. W. *Chem. Commun*. **1997**, 1607.

[13] For an example of each structure type see: (a) Caulton, K. G.; Chisholm, M. H.; Drake, S. R.; Folting, K. *Chem. Commun.* **1990**, 1349. (b) Holl, M. M. B.; Wolczanski, P. T. *J. Am. Chem. Soc.* **1992**, *114*, 3854. (c) Koide, Y.; Barron, A. R. *Organometallics*, **1995**, *14*, 4026. (d) Karet, G. B.; Sun, Z.; Heinrich, D. D.; McCusker, J. K.; Folting, K.; Streib, W. E.; Huffman, J. C.; Hendrickson, D. N.; Christou, G. *Inorg. Chem.* **1996**, *35*, 6450. (e) Fandos, R.; Hernandez, C.; Otero, A.; Rodriguez, A.; Ruiz, M. J.; Garcia Fierro, J. L.; Terreros, P. *Organometallics* **1999**, *18*, 2718. (f) Yuki, M.; Okazaki, M.; Ogino, H. *Chem. Lett.* **1999**, 649. (g) Han, J.; Koutmos, M.; Al Ahmad, S.; Coucouvanis, D. *Inorg. Chem.* **2001**, *40*, 5985. (h) Fromm, K. M.; Gueneau, E. D.; Bernardinelli, G.; Goesmann, H.; Weber, J.; Mayor-Lopez, M. –J.; Boulet, P.; Chermette, H. *J. Am. Chem. Soc.* **2003**, *125*, 3593. (i) Sadr, M. H.; Clegg, W.; Bijhanzade, H. R. *Polyhedron* **2004**, *23*, 637.

[14] For an example see: Jones, R. A.; Stuart, A. L.; Wright, T. C. *J. Am. Chem. Soc.* **1983**, *105*, 7459.

[15] Hill, R. J.; Long, D. –L.; Champness, N. R.; Hubberstey, P.; Schröder, M. *Acc. Chem. Res.* **2005**, *38*, 335.

[16] Schriver, D. F.; Drezdon, M. A. *The Manipulation of Air-Sensitive Compounds*, Wiley, New York, **1986**.

[17] Chisholm, M. H.; Drake, S. R.; Naiini, A. A.; Streib, W. E. *Polyhedron* **1991**, *10*, 337.

[18] Edelmann, F. T.; Pauer, F.; Wedler, M.; Stalke, D. *Inorg. Chem*. **1992**, *31*, 4143.

[19] J. Kaercher, *COSMO,* Bruker-Nonius AXS, Inc., Madison, Wisconsin, USA, **2003**.

[20] G. M. Sheldrick, University of Göttingen, Göttingen (Germany), **2001**.